Biomaterials 139 (2017) 116–126

Contents lists available at ScienceDirect

Biomaterials

journal homepage: www.elsevier.com/locate/biomaterials

Targeting epithelial-mesenchymal transition: Metal organic network nano-complexes for preventing tumor metastasis

Jin-Xuan Fan [a, 1], Di-Wei Zheng [a, b, 1], Lei Rong [a], Jing-Yi Zhu [a], Sheng Hong [a], Cao Li [b], Zu-Shun Xu [b], Si-Xue Cheng [a], Xian-Zheng Zhang [a, *]

[a] Key Laboratory of Biomedical Polymers of Ministry of Education, Institute for Advanced Studies (IAS), Department of Chemistry, Wuhan University, Wuhan, 430072, PR China

[b] Hubei Collaborative Innovation Center for Advanced Organic Chemical Materials, Key Laboratory for the Green Preparation and Application of Functional Materials of Ministry of Education, Hubei University, Wuhan, Hubei, 430062, PR China

ARTICLE INFO

Article history:
Received 28 May 2017
Accepted 4 June 2017
Available online 6 June 2017

Keywords:
Epithelial-mesenchymal transition
Tumor metastasis
Multidrug resistance
Nano-medicine
Anti-cancer therapy

ABSTRACT

Tumor metastasis is the leading cause of death in cancer patients, and epithelial-mesenchymal transition (EMT) is an essential step in tumor metastasis. Unfortunately, during the chemotherapy, EMT could be induced under the selective pressure of clinical cytotoxic drugs. Here, to solve this problem, we have synthesized multi-functional epigallocatechin gallate/iron nano-complexes (EIN) as a versatile coating material to improve conventional therapies. *In vitro* studies showed that this strategy could eliminate EMT-type cancer cells. Mechanism studies also revealed that EIN was able to down-regulate the downstream expression of metastasis-associated factors, decrease the migration ability of cancer cells and prevent cancer cells from gaining drug resistance. *In vivo* investigation revealed that EIN had superior ability to enhance the therapeutic effect of conventional nanomedicines and inhibit the EMT process. Our study indicates the promising use of EIN to make up for the deficiencies of chemotherapy may provide insights into systematic cancer therapy to overcome tumor metastasis and drug resistance.

1. Introduction

Tumor metastasis is the leading cause of the high mortality of cancers with poor prognosis [1]. Despite recent advances in tumor treatments, therapeutic methods for tumor metastasis treatments are still very limited. Recently, a range of strategies have been proposed to fight against tumor metastasis. Among them, designing metastatic tumor targeting materials is a promising method to treat advanced cancers. However, this strategy is restricted by limited differences between metastatic tumors and primary tumors [2,3]. In earlier studies, researchers mainly focused on the capture of circulating tumor cells. Nevertheless, to eliminate all circulating tumor cells in the whole circulatory system remains a great challenge and few escaped circulating tumor cells could cause serious distant metastasis [4,5]. To date, increasing evidences have suggested that tumor microenvironment (TME) normalization strategies such as tumor oxygenation, acidic environment neutralization and drug resistance reversion are effective solutions for metastasis prevention. Besides, various nanomaterials such as g-C_3N_4 nanoparticles, MnO_2 nano-sheets and metal-organic frameworks have been used to alleviate tumor hypoxia and neutralized acidic environment [6–9]. Therefore, an ideal material for effective metastasis prevention should have satisfactory performance in TME normalization [10,11].

As it is well known, with the effect of chemotherapeutic agents, cancer cells would undergo adaptive changes and update their drug resistance ability, which make chemotherapeutic agents less effective [12]. Emerging evidences also demonstrate that the development of drug resistance could induce specific variations, which are consistent with EMT, a dominant step involves in tumor metastasis [13–15]. Furthermore, cancer cells which undergo EMT, would up-regulate the expression of metastatic factors including matrix metalloproteinase (MMP) and vascular endothelial growth factor (VEGF) to induce extracellular matrix degradation and trigger neovessel formation [16]. These changes could provide escape routes for cancer cells to leave the primary tumor and spread to other organs such as lung and liver [17]. As a consequence, to eliminate EMT type cancer cells that with both

* Corresponding author.
E-mail address: xz-zhang@whu.edu.cn (X.-Z. Zhang).
[1] J.X.F. and D.W.Z. contributed equally to this work.

http://dx.doi.org/10.1016/j.biomaterials.2017.06.007
0142-9612/

intensified drug resistance and high metastatic capability is of great importance during chemotherapy.

Traditionally, small molecule inhibitors were used to overcome drug resistance. However, the non-specific inhibition of P-glycoprotein (P-gp) would frequently increase side effects of chemotherapeutics due to the compromised drug elimination in liver and kidney. Nano-carries have been demonstrated to enhance the therapeutic effect of small molecule agents by improving the tumor targeting capability and reducing the side effect *via* their enhanced permeability and retention (EPR) effect [18–20]. Thus, designing a nanomedicine to inhibit the development of drug resistance within primary tumor would be a superior way to overcome the shortcoming of traditional inhibitors.

Tea polyphenols are a series of compounds found in tea. A FDA approved tea polyphenol, epigallocatechin gallate (EGCG), is found to surmount drug resistance through modulating of cell signaling and finally down-regulate the expression of P-gp [21,22]. Previous studies show that catechol containing molecules could assemble with metal ions to prepare versatile films for nanoparticles coating [23–26]. Keeping all these issues in mind, in this work, we constructed a functional coating membrane through coordinating epigallocatechin gallate (EGCG) with ferric ions to prepare epigallocatechin gallate/iron nano-complexes (EIN) with ideal biocompatibility and low cytotoxicity.

Furthermore, as a universal coating material, EIN was used to coat traditional drug delivery nanoparticles such as mesoporous silica nanoparticles (MSN) and PEG-PLA micelles (Mic) to form MSN@EIN and Mic@EIN, respectively. Inherited from EGCG, MSN@EIN and Mic@EIN showed a high capability to enhance the intracellular drug concentration and to prevent drug resistance during chemotherapy. According to previously studies, although the combined administration of free EGCG and free doxorubicin (DOX) could also prevent cancer cells from gaining drug resistance, significant toxicity to liver and kidney could not be neglected as revealed by blood biochemical analysis. Herein, DOX@MSN@EIN and DOX@Mic@EIN drug delivery systems were prepared to avoid the shortcoming of small molecule inhibitors with minimized liver and kidney toxicity. In the follow up study, we disclosed that EIN also eliminated EMT-type cells and restricted the tumor metastasis *in vitro* and *in vivo*. Detailed mechanism studies demonstrated that the presence of MSN@EIN and Mic@EIN in the drug delivery systems notably inhibited drug resistance and eliminated EMT-type cells. Besides, the inhibited EMT process of cancer cells further down-regulated the expression of metastasis factors such as matrix metalloproteinases (MMP) including MMP-2/9 and VEGF. Overall, EIN encapsulation is a versatile and universal method for upgrading current nanomedicines, which provides a novel strategy to develop anti-cancer agents.

2. Materials and methods

2.1. Materials

Methanol, dimethyl formamide (DMF), sodium hydroxide (NaOH), triethylamine (TEA), dimethyl sulfoxide (DMSO), dichloromethane, hydrochloric acid (HCl), ethylsilicate (TEOS), hexadecyl trimethyl ammonium bromide (CTAB), and hydrofluoric acid were purchased from Shanghai Reagent Chemical Co. H_2O_2, tris-(hydroxymethyl) aminomethane (Tris), (−)-epigallocatechin-3-gallate (EGCG) and ferric (III) chloride hexahydrate ($FeCl_3 \cdot 6H_2O$) were from Aladdin Industrial Corporation. Ferrous lacate (edible grade) was purchased from Zhengzhou Hongxiang Chemical Co. Ethylene diamine tetraacetic acid (EDTA), Tween 20, catalase and urea were supplied by Sigma-Aldrich. PEG_{2000}-PLA_{2000} was obtained from Xian Ruixi Biological Technology Co., Ltd. Toluene, DMF and TEA were redistilled before used. Doxorubicin hydrochloride (DOX) was provided by Zhejiang Hisun Pharmaceutical Co. (China). Antibodies were obtained from Abcam and Bioss.

2.2. Preparation of DOX@MSN

1.0 g of CTAB (274 mM) and 280 mg of NaOH (7 mM) were dissolved in 480 mL of DI water and kept at 80 °C for 0.5 h. Then 5.0 g of TEOS (24 mM) was added dropwise for 20 min under vigorous stirring. After 2 h, the resulting product was centrifuged (10,000 r/min, 15 min), and washed with DI water and methanol for three times. Then, the mixture of 200 mg of CTAB@MSN, 80 mL of methanol and 5 mL of HCl was refluxed at 80 °C for 48 h. The resulting product was centrifuged (10,000 rpm, 15 min), and washed with methanol and water several times. After that, 100 mg of MSN was suspended in a methanol/H_2O mixture with 20 mg of DOX (36.8 μM) and stirred for 24 h. The product was washed with methanol and water, and then lyophilized for 3 days.

2.3. Preparation of DOX@Mic

5 mg DOX (9.2 μM) (desalt) and 50 mg PEG-PLA were dissolved in 2 mL dichloromethane in a round-bottom flask. The solvent was evaporated by rotary evaporation at room temperature under vacuum to obtain DOX@Mic. The product was dissolved in DI water and dialyzed for 2 days.

2.4. Preparation of DOX@MSN@EIN and DOX@Mic@EIN

5 μL of polyphenol solution (1 mM) and 5 μL of $FeCl_3.6H_2O$ (1 mM) solution were added to 500 μL of DOX@MSN or DOX@Mic containing solution (0.1 mg/mL), respectively. The mixture was vigorously mixed under ultrasonication for 30 s immediately after the individual additions of polyphenol and $FeCl_3 \cdot 6H_2O$. The pH value of this mixture was then raised to 8.0 by adding 0.5 mL of tris buffer (20 mM, pH 8.5). The product was dialyzed against water for 2 days to obtain EIN coated nanoparticles.

2.5. Cell culture and in vitro toxicity

The cell toxicity was examined by MTT assay. 4T1 cells was seeded in a 96-well plate with a cell density of 5×10^4 per well, and then incubated in 100 μL of cell culture medium containing 10% FBS in an incubator (37 °C, 5% CO_2) for 24 h. The medium containing a particular agent was added to each well respectively. After 48 h, the cells were washed with EDTA to remove the Fe^{3+}. After that, the medium was replaced with 200 μL of fresh medium and 20 μL of MTT (5 mg/mL in PBS buffer) was added. After incubation at 37 °C for 4 h, the medium was removed and 150 μL of DMSO was added. The absorbance was measured at 570 nm using a microplate reader (Bio-Rad, Model 550, USA). The relative cell viability was calculated by ($OD_{570sample}/OD_{570control}$) × 100%, where $OD_{570control}$ was obtained in the absence of the agent and $OD_{570sample}$ and in the presence of the agent.

2.6. Cellular uptake

Cells were seeded in a small plate with a density of 1×10^5, and incubated with 1 mL of medium containing 10% FBS at 37 °C for 24 h. 1 mL of medium containing a particular agent was added. After incubated with cells for 4 h, the medium was removed and cells were washed three times. Then cells were observed with CLSM. (Nikon C1-si, TE2000, Japan).

2.7. In vitro MDR reversion study

MCF-7/ADR cells were seeded in a small plate with a density of 1×10^5 well and incubated overnight. The cells were washed and treated with free DOX or DOX contained EIN coated nanomedicines at a concentration of 5 μg/mL. After 4 h of co-incubation, the cells were washed twice with cold PBS, and observed by CLSM. Then, cells were incubated with culture medium at 37 °C for an additional 24 h, and the cells were observed by CLSM at different time points.

2.8. In vitro MDR and EMT prevention studies

4T1 cells were seeded in a small plate with a density of 1×10^5 cells/well and incubated overnight. The cells were washed and treated with free DOX or DOX contained EIN coated nanomedicines with their IC_{50} concentration. After 24 h of co-incubation, cells were washed twice with cold PBS, and treated with 5% BSA for 30 min at room temperature, and then stained with rabbit anti-mouse P-gp, rabbit anti-mouse vimentin or rabbit anti-mouse E-cadherin primary antibody (1:100; Cell Signaling) at 4 °C overnight. Cells were incubated with goat anti-rabbit FITC secondary antibody (Abcam), diluted (1:200) in PBS, for 2 h at 4 °C, and then washed with PBS. Then, cells were incubated for 10 min at room temperature with DAPI (1:10,000; Sigma) to stain nuclei, washed twice with PBS, and observed by CLSM.

2.9. In vivo biodistribution study

After subcutaneous tumors reached about 6 mm in diameter, *in vivo* DOX fluorescence imaging was performed on a Maestro imaging system (CRi, Inc, Woburn, MA). For the distribution analysis, various materials were injected through a tail vein with a DOX does of 5 mg/kg. After the injection for 24 h, mice were sacrificed. Images of heart, liver, spleen, lung kidney and tumor were obtained by using a set of filters specifically for DOX imaging.

2.10. In vivo MRI study

The EIN containing solution with different iron concentrations were diluted with DI water ultrasonically and obtain a final iron concentration in the range of 0.1 to 0.0625 mM. Then, samples were transferred into NMR tubes and placed in a 7.0 MR scanner. The T1 relaxation time of the sample was computed using Paravision 5.0. The T1 relaxation rate (1/T1) was plotted versus the Fe concentration and the T1 relaxivity was calculated based on a linear fit. The *in vivo* MRI imaging experiment was performed on Balb/c mice weighting approximately 15 g. Mice were anaesthetized by isoflurane before *i.v.* injected. Then, mice were scanned before and after injection of 0.1 mL of DOX@MSN@EIN containing solution at a dose of 0.5 mg [Fe]/kg body weight. The T1-weighted MR image of the tumor was obtained on a 7.0 T MR scanner.

2.11. Ex vivo metabonomics study

4T1 tumor tissue was extracted by using 1 mL of 50% acetonitrile/50% D_2O. Preweighed tissue (200 mg) was homogenized in the solvent above, and then was centrifuged at 10,000 rpm for 6 min. After that, the supernatant was collected and evaporated to get the solid product. The product was dissolved in 0.5 mL of D_2O prior to NMR analysis. For each group, equal amount of phenylsulfonic acid was added as an internal standard. Following the NMR spectral phase and baseline correction, the NMR dates were data-reduced to 256 regions of equal width (0.04 ppm) and integration using the Mestnove software package, version 2.0 (Bruker Biospin).

2.12. In vitro Boyden chamber assay

4T1 cells were pretreated with MSN@EIN and Mic@EIN at 40 μg/mL for 24 h. 100 μL of Matrigel (1 mg/mL) was coated to 8 μm transwell cell culture inserts, while 100 μL of standard medium was placed in the bottom chamber. Then, cells were harvested and seeded in inserts at 5×10^4 cells/well in serum-free medium and then incubated for 48 h at 37 °C. After that, crystal violet was used to stain the cells in 24 well plates. Metastatic cells were imaged and counted with Image J.

2.13. Western blot and RT-PCR studies

For WB analysis, cell lysate was treated with 50 μL of RIPA buffer and resuspended in 50 μL of SDS buffer with 1% β-mercaptoethanol. Then the samples were heated for 5 min and separated on a 10% SDS-PAGE (15 μL per lane). After electrophoresis, proteins were transferred to a PVDF membrane (Millipore). PVDF membranes were then blocked in PBS with 5% skim milk for 1 h. MMP-2, MMP-9, VEGF, E-cadherin, vimentin, P-gp and GST-π were detected. The membranes with the primary antibody rabbit anti-mice antibody (1:2000 dilution) overnight at 4 °C and then with the secondary antibody HRP labeled goat antirabbit IgG (1:3000 dilution, KPL) for 1 h. Specific proteins were monitored by enhanced chemiluminescence. GADPH antibody (Abcam, Rabbit) was employed as protein loading control.

For RT-PCR analysis, RNA of cells was extracted. The RNA samples were reverse-transcribed to cDNA using a first stand cDNA synthesis kit (TOYOBO, Japen). The relative expression of MMP-2, MMP-9 and VEGF was then measured *via* real-time PCR using a StepOne™ Real-Time PCR (Life technologies, USA). Specific primers for the genes were provided by Invitrogen. Each PCR reaction was performed in 10 μL of a reaction mixture containing 5.0 μL of 2 × qPCR Mix, 1.0 μL of each primer, 1.0 μL of template, 2.8 μL of DI water and 0.2 μL of rox. The samples were then subjected to cycling conditions as the protocol specified in the SYBR® Premix Ex Taq gene expression assay kit. The level of expression of the gene, normalized to GAPDH, was then calculated using the ΔΔCT formula.

2.14. Immunofluorescence and immunohistochemical (IHC) studies

For immunofluorescence and IHC studies, tumor samples were collected, and rinsed with cold PBS and immediately frozen at −80 °C. Tissue slices were prepared by means of a frozen section machine. After blocking non-specific binding of antibody with 10% fetal calf serum (FCS) (1 h), samples were stained with primary antibodies specific for MMP-2, MMP-9, VEGF, E-cadherin, vimentin, P-gp and GST-π in a humidified chamber for 2 h. Then, the samples were washes with 10% FCS for 3 times, and FITC or Cy-5.5 conjugated appropriate secondary antibodies (Molecular Probes-Life Technologies Inc) (5 μg/mL) were added. Nuclei were stained with 10 μM DAPI. Coverslides were mounted with Fluoromount-GTM medium (Southern Biotechnologies). CF350 conjugated Top-2a antibody was used to visualize the Top-2a. Slices are imaged with an LSM 710 Confocal Microscope (Zeiss, Jena, Germany). Quantitative study of immunofluorescence staining and fluorescent colocalization analysis was performed with Image J.

2.15. In vivo anti-cancer efficacy

All the animal experiments were performed according to the guidelines for laboratory animals established by the Wuhan University Center for Animal Center Experiment/A3-Lab. Female balb/c mice were subcutaneously injected with 4T1 cells (5×10^6 cells/mouse). After the tumor volume reached to 100 mm^3, mice were

randomized divided into 8 groups with 7 mice each. Then, mice were *i.v.* injected with 100 μL of DOX loaded materials (with a DOX concentration of 5 mg/kg), DOX (5 mg/kg) and EGCG (5 mg/kg) at 1st and 20th days. The volume was defined as: $V = (L \times W^2)/2$. Relative tumor volume was defined as V/V_0 (L is the tumor length, W is the tumor width and V_0 is the tumor volume when the treatment was initiated). After 25 days of treatment, mice were sacrificed. H&E staining, immunofluorescence staining and immunohistochemistry (IHC) were used for further examinations. In order to examine lung metastasis, mice was sacrificed and India ink (15%) was injected through the trachea. Livers were collected and photographed immediately, and white spots on the lungs (tumor metastasis) were counted.

2.16. In vivo MDR reversion study

Human MCF-7/ADR tumor xenografts were established in female Balb/c nude mice. Mice were subcutaneously injected with 1×10^6 of MCF-7/ADR cells. In order to support the growth of the estrogen-dependent MCF-7 tumors, (17β)-estra-1,3,5(10)-triene-3,17-diol17-cyclopentanepropanoate (estradiol cypionate injection, USP) was intramuscularly injected with a dosage of 3 mg/kg per weeks. After the tumor volume had reached 100 mm^3, mice were randomized divided into 7 groups with 5 mice each. Then, mice were *i.v.* injected with 100 μL of DOX loaded materials (with a DOX concentration of 5 mg/kg) and DOX (5 mg/kg) at 1st and 7th days. Tumor volume and mice weight were recorded once a day. After 15 days of treatment, mice were sacrificed. Tumors were imaged and H&E staining was performed.

3. Results and discussion

3.1. Preparation and characterization of EIN coated drug delivery systems

Herein, DOX was loaded in MSN or Mic first, EIN coating was performed with a one-pot synthesis method (Scheme 1). And the detail of EIN formation was showed in Fig. 1A. TEM images of MSN, Mic and EIN coated nanoparticles are shown in Fig. 1B–E, respectively. Particle sizes and zeta potentials of DOX@MSN@EIN and DOX@Mic@EIN in water were found to be 198 nm/-28.4 mV and 245 nm/-27.5 mV, respectively (Tables S1 and S2). The DOX loading levels of DOX@MSN@EIN and DOX@Mic@EIN were calculated to be 2.2% and 8.4%, respectively. The EGCG loading levels of DOX@MSN@EIN and DOX@Mic@EIN were calculated to be 1.1% and 1.4%. Furthermore, the driving force for the EIN formation was investigated by the addition of Tween 20, urea, ethylenediaminetetraacetic acid (EDTA) and sodium chloride (NaCl). EIN was effectively dissociated by EDTA as a result of coordinate competition, while Tween 20, urea and NaCl were ineffective in inducing EIN dissociation (Fig. S1). These results indicated that EIN was constructed through coordinate bonds, rather than hydrophobic interactions, hydrogen bonds, or ionic interactions [27]. Moreover, the formation of coordinate bonds between polyphenol and Fe^{3+} was also confirmed by FT-IR and XPS (Figs. S2 and S3).

3.2. In vitro stimuli-responsive drug release and cytotoxicity

Previously, it has been found that the coordination between Fe^{3+} and polyphenols is pH-dependent. Under low pH, EGCG/Fe^{3+} coating layer degrades due to destruction of the coordination structure which leads to the drug release [28]. Besides, polyphenol was reported to gradually degrade with the participation of H_2O_2 (Fig. S4A). We studied the stimuli-responsive drug release property of EIN based drug carriers. As shown in Fig. S4B$_1$–B$_2$, at pH = 5.6 with 25 μM H_2O_2, EIN could release 95% of the loading drug within 24 h. Whereas, only limited amount of loaded DOX (less than 40%) was released within 24 h at pH = 7.4/25 μM H_2O_2 or pH = 5.6/0 μM H_2O_2, and less than 20% of loaded DOX was released in neutral condition without H_2O_2.

MTT assay was used to evaluate the *in vitro* anti-cancer ability of DOX@MSN@EIN and DOX@Mic@EIN. As shown in Fig. 2A, significant cytotoxicity of DOX@MSN@EIN and DOX@Mic@EIN in 4T1 cells was observed, and IC_{50} values were calculated to be 0.89 μg/mL and 0.91 μg/mL (DOX concentration), respectively. In this study, catalase and NH_4Cl were respectively added to induce H_2O_2 depletion and intracellular pH restoration [29]. As shown in Fig. 2B, after treated with catalase and NH_4Cl, cytotoxicities of DOX@MSN@EIN and DOX@Mic@EIN toward 4T1 cells were suppressed.

Furthermore, confocal laser scanning microscopy (CLSM) was used to visualize the cellular uptake of various nanoparticles (Fig. 2C and D). After the co-incubation of DOX@MSN@EIN and

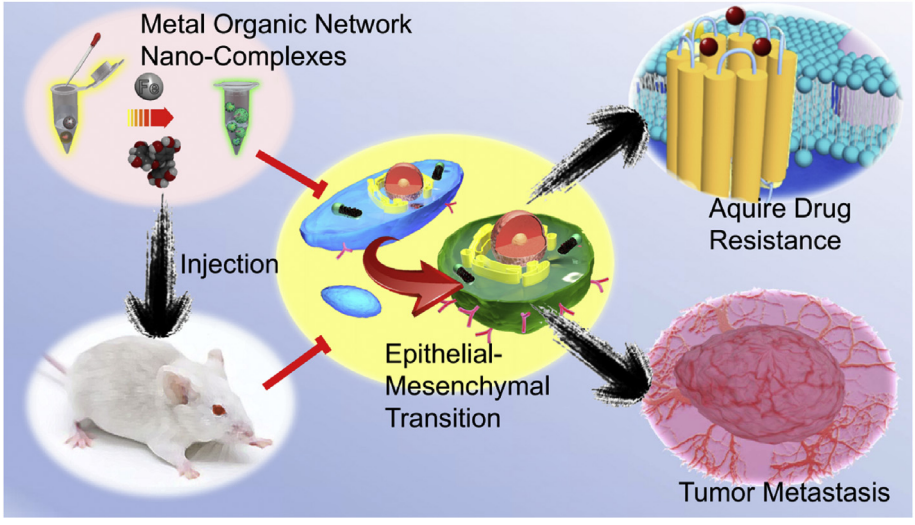

Scheme 1. Schematic diagram of the EIN coated nanomedicines to prevent cancer cells from gaining drug resistance and eliminate EMT-type cancer cells for inhibiting tumor metastasis.

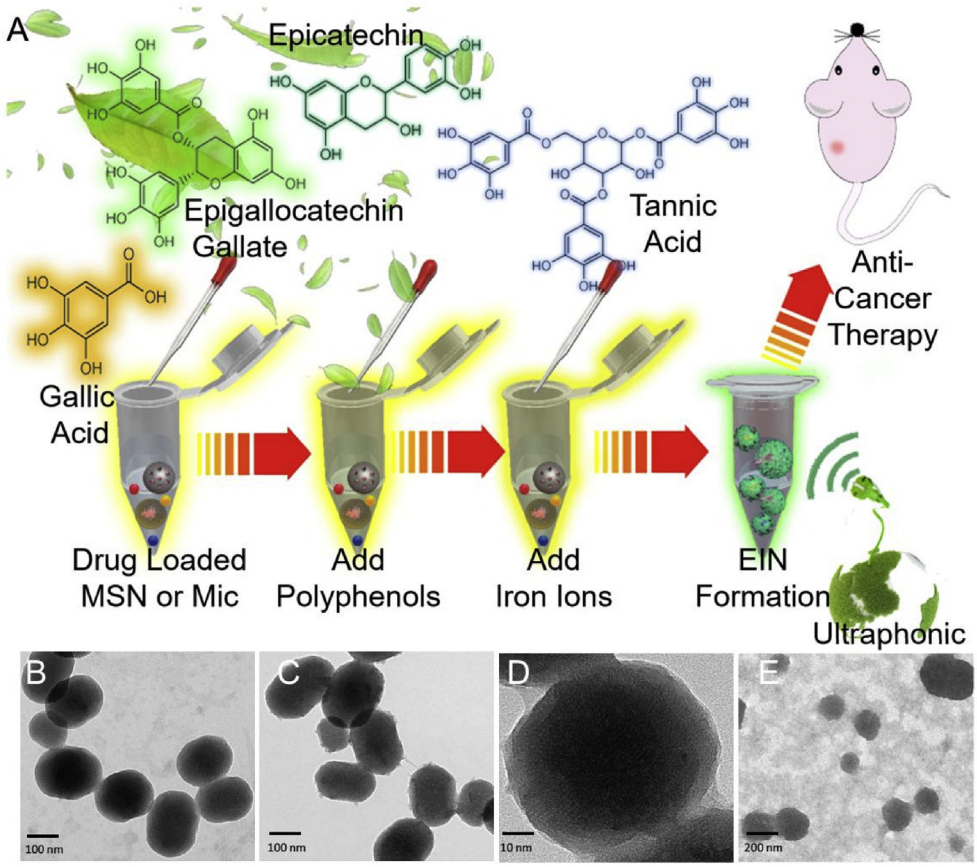

Fig. 1. The schematic representation for nanoparticle synthesis (A). DOX was loaded in MSN or Mic first, polyphenols and iron ions were added subsequently to perform EIN coating with a one-pot synthesis method. TEM images of (B) DOX@MSN, (C–D) DOX@MSN@EIN and (E) DOX@Mic@EIN.

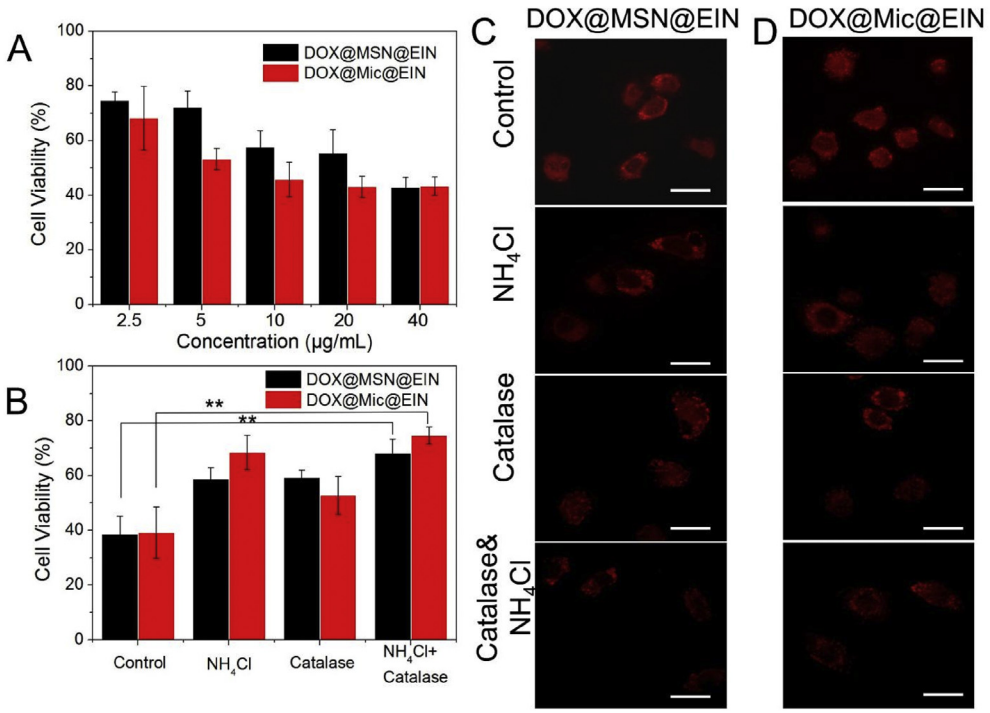

Fig. 2. (A) Cell viability assay of DOX@Mic@EIN and DOX@MSN@EIN treated 4T1 cells. (B) Cell viability assay of DOX@Mic@EIN and DOX@MSN@EIN treated 4T1 cells after co-incubated with NH_4Cl and catalase. (C–D) CLSM images of DOX@MSN@EIN and DOX@Mic@EIN treated 4T1 cells after co-incubated with NH_4Cl and catalase. (Scale bar: 10 μm).

DOX@Mic@EIN with 4T1 cells for 8 h, DOX fluorescence was eventually accumulated in the nucleus region, mainly because free DOX intended to accumulate in the nuclei by formation of DOX-proteasome complexes. In contrast, after treated with NH_4Cl or catalase, which prevented EIN from degrading, most of red fluorescence of DOX was distributed in the cytoplasm, and limited amount of fluorescence was accumulated in the nucleus region. This result indicated that the drug release from EIN coated nanoparticles was triggered by the intracellular low pH and high H_2O_2 level [30].

3.3. *In vitro drug resistance prevention and drug resistance reversion*

It is well known that during chemotherapy, cancer cells would undergo adaptive changes and gain drug resistance, which made cancer cells relatively invulnerable to various cytotoxic anti-cancer agents [31]. As shown in Fig. S5, RT-PCR detection indicated that remarkably increased *MDR1* gene after the co-incubation of DOX and 4T1 cells, which demonstrated the induced drug resistance of 4T1 cells. Whereas the addition of EGCG significantly suppressed the transcription of *MDR1* gene. Furthermore, we observed that DOX@MSN@EIN and DOX@Mic@EIN could also prevent 4T1 cells from gaining drug resistance. As shown in Fig. 3A, EMT process was accompanied with the decrease of vimentin (a mesenchymal marker) and the increase of E-cadherin (an epithelial marker). The DOX treatment not only resulted in the updating of drug resistance, but also induced EMT in epithelial 4T1 cells, as well as increased vimentin level and decreased E-cadherin expression. Gray-scale analysis of protein bands revealed 94% and 78% increases in DOX-induced P-gp and vimentin expression in 4T1 cells, and 64% decrease in E-cadherin expression. Therefore, DOX + EGCG,

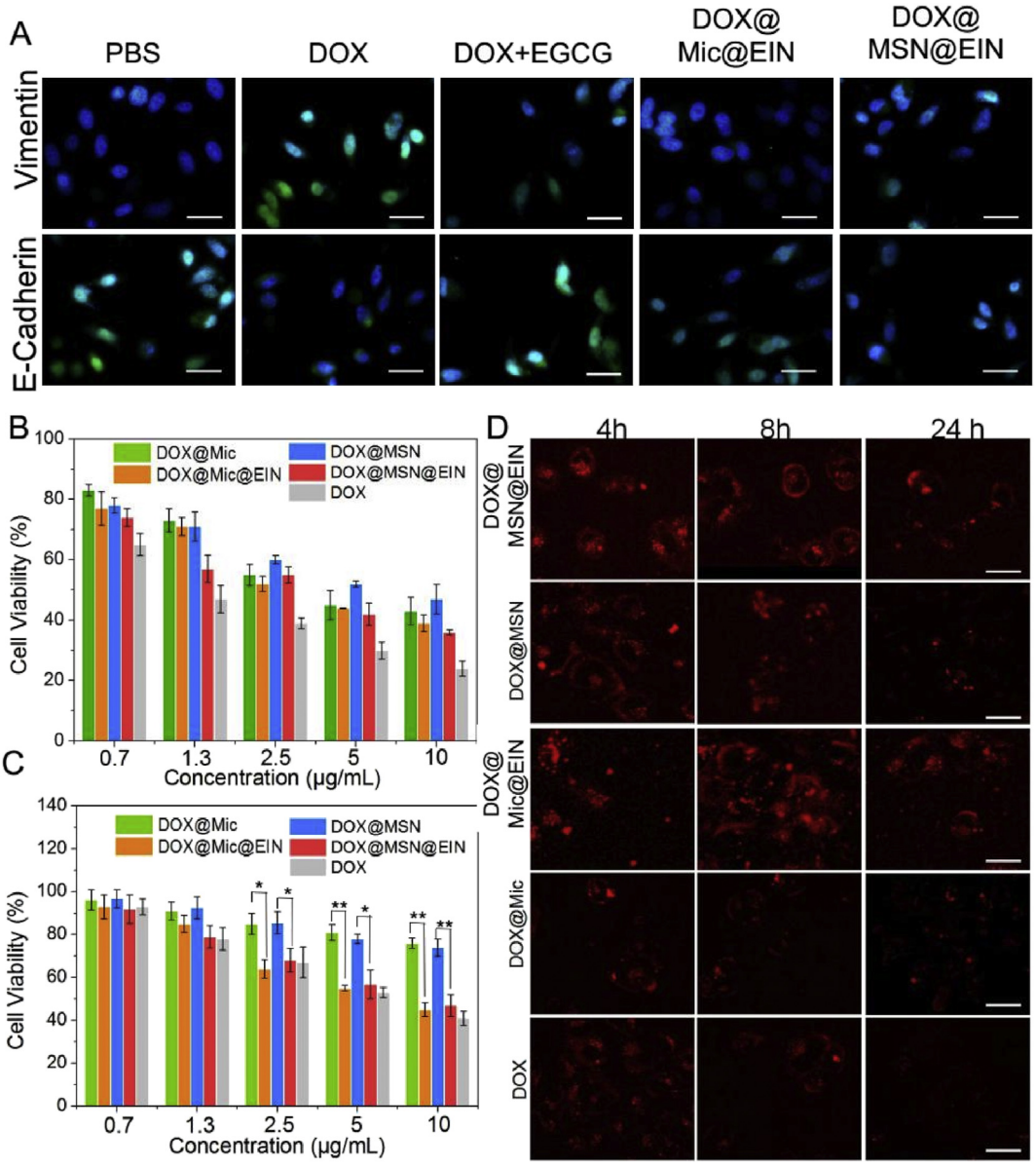

Fig. 3. (A) P-gp, vimentin and E-cadherin immunofluorescence images of 4T1 cells after co-incubation with PBS, DOX, DOX@EGCG, DOX@Mic@EIN and DOX@MSN@EIN. (Scale bar: 10 μm) (B) Cell viability assay on free DOX, DOX@MSN, DOX@Mic, DOX@Mic@EIN and DOX@MSN@EIN treated 4T1 cells. (C) Cell viability assay on free DOX, DOX@MSN, DOX@Mic, DOX@Mic@EIN and DOX@MSN@EIN treated MCF-7/ADR cells. (D) CLSM images of MCF-7/ADR cells pretreated with free DOX, DOX@MSN, DOX@Mic, DOX@Mic@EIN and DOX@MSN@EIN for 6 h with additional incubation with fresh culture medium for 4, 8, and 24 h, respectively. (Scale bar: 10 μm).

DOX@MSN@EIN and DOX@Mic@EIN treatments could prevent both the acquisition of drug resistance and the subsequent induced EMT process *in vitro*.

After that, the drug resistance reversion of MCF-7/ADR cells was studied. The anti-proliferation efficiency of EIN coated nanomedicines against MCF-7/ADR cells was tested by MTT assay [32,33]. As shown in Fig. 3B and C, the IC_{50} value of free DOX for MCF-7/ADR cells was 5.3 μg/mL. Whereas, the IC50 values of DOX@MSN@EIN and DOX@Mic@EIN were 8.3 and 7.8 μg/mL for MCF-7/ADR cells, respectively. Besides, the drug resistance factors of DOX@MSN@EIN and DOX@Mic@EIN were 2.3 (calculated as 8.1/3.5) and 2.4 (calculated as 7.4/3.1), respectively, which were lower than that of free DOX (5.4, calculated as 6.3/1.2). Generally speaking, drug loaded in nanoparticles is hard to be released completely and effect onset rapidly compared with free drug, which cause free drug has lower IC50 compared to nanoparticles. Thus, this result validated the robust anti-drug resistance capability of EIN coated nanomedicines.

Then, CLSM images of free DOX, DOX@MSN, DOX@Mic, DOX@MSN@EIN and DOX@Mic@EIN treated MCF-7/ADR cells are shown in Fig. 3D. Cells treated with DOX@MSN@EIN and DOX@Mic@EIN exhibited stronger red fluorescence. The quantitative analysis of DOX fluorescence in Fig. S6 indicated that EIN coated materials could efficiently enhance the concentration of anticancer drugs in drug resistant cancer cells. Cytotoxicity study on MCF-7/ADR cells also confirmed that EIN could avoid drug resistance in drug resistant cancer cells. Clearly, this was attributed to the down-regulated P-gp expression in cancer cells after treated with DOX@MSN@EIN and DOX@Mic@EIN.

3.4. In vitro anti-metastasis study

After confirming the mechanism of DOX@MSN@EIN and DOX@Mic@EIN in preventing cancer cells from gaining drug resistance and eliminating highly drug resistant EMT type cells, the influence of EIN on cell invasion, and metastasis associated morphology changes was investigated. The adhesion of cancer cells to a distant location is a key process of cancer metastasis, thus, cell-matrix adhesion assay and wound-healing migration assay were performed as well (Fig. 4A and B). Compared to PBS, MSN or Mic treated samples, the decreased cell count in cell-matrix adhesion assay and the increased average distance in wound-healing migration assay of EIN treated samples confirmed the preferable anti-migration ability (Fig. S7).

In addition, the metastasis restriction of EIN was also studied by

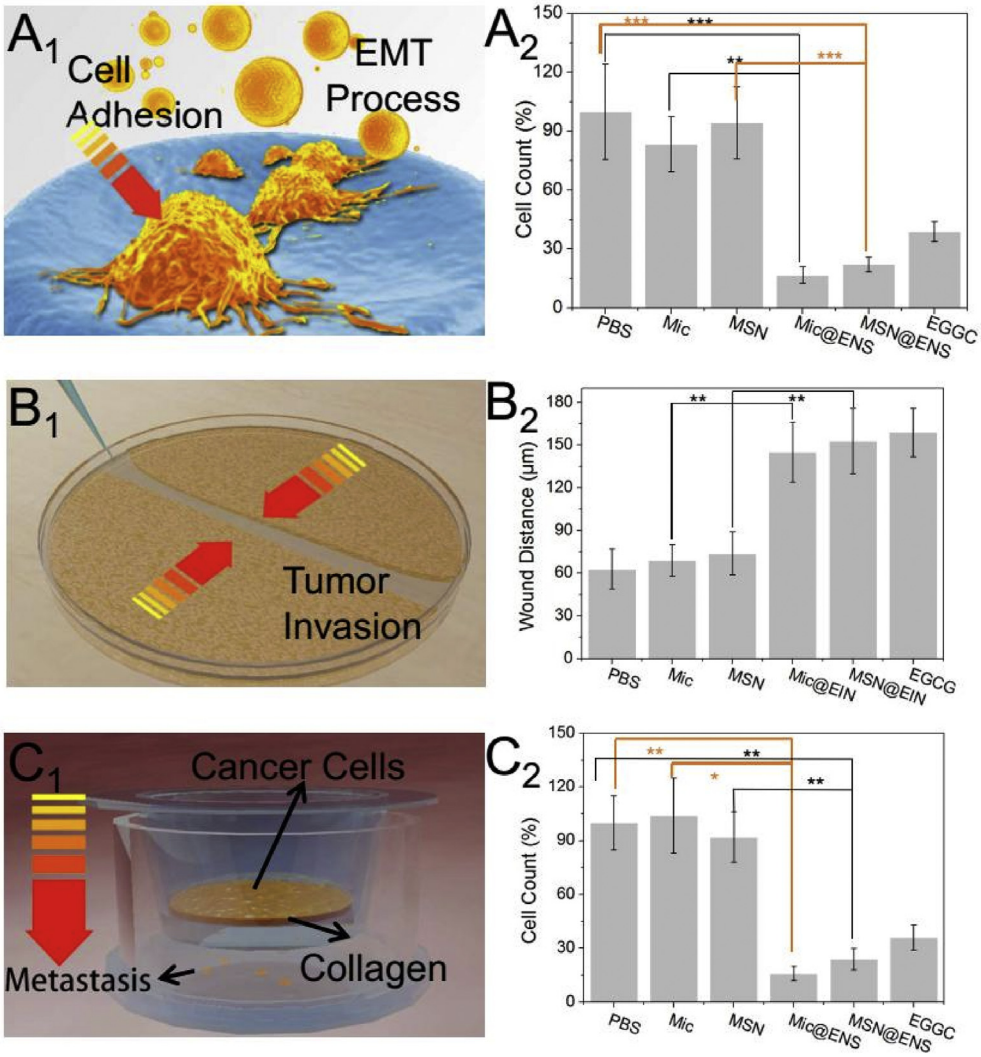

Fig. 4. (A) Cell adhesion assay of 4T1 cells after co-incubated with PBS, DOX@Mic, DOX@MSN, DOX@Mic@EIN and DOX@MSN@EIN. (B) Wound healing assay of 4T1 cells after co-incubated with PBS, DOX@Mic, DOX@MSN, DOX@Mic@EIN and DOX@MSN@EIN. (C) Boyden chamber assay of 4T1 cells after co-incubated with PBS, DOX@Mic, DOX@MSN, DOX@Mic@EIN and DOX@MSN@EIN.

collagen coated Boyden Chamber assay (Fig. 4C). Herein, after treated with MSN@EIN or Mic@EIN for 24 h, the number of 4T1 cells migrated through collagen was counted. MSN@EIN and Mic@EIN treatments could reduce 84% and 78% of 4T1 cells migration, respectively, which indicated the satisfactory metastasis restricting capability of these complexes. Metastasis is a complicated event starting with tumor micro-environment modulated degradation of extracellular matrix (ECM), during which the expression of MMP-2 and MMP-9 play an importance role. Hereby, the expression of MMP-2/9 and VEGF in 4T1 cells after co-incubated with various materials was determined. As shown in Fig. S8, down-regulated MMP-2/9 and VEGF levels were definitely observed after MSN@EIN and Mic@EIN treatments. In the meantime, P-gp and GST-π levels reduced appreciably as well. Thus, we suggest that the metastatic capability of tumor could also be inhibited by using this strategy. In addition, low *in vitro* cytotoxicity and satisfactory blood compatibility of EIN in various concentrations are favorable for *in vivo* applications (Fig. S9).

3.5. In vivo anti-cancer therapy

The anti-cancer capability of EIN coated nanomedicines was investigated *in vivo*. And the anti-cancer efficiency was evaluated by toxicology, pathology, metabonomics and protein analysis (Fig. 5A).

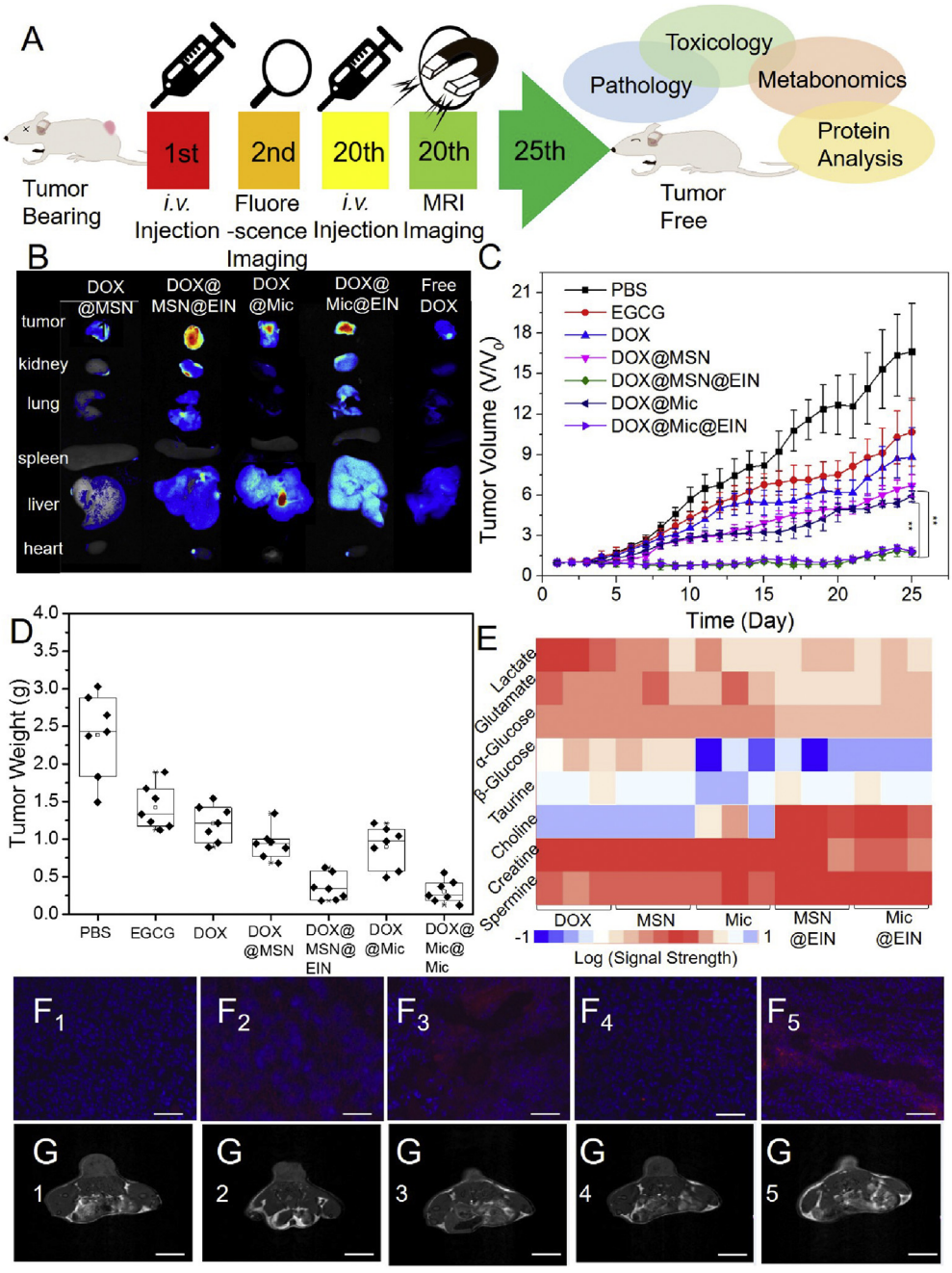

Fig. 5. (A) Schematic diagram of experimental setups. (B) *Ex vivo* fluorescence imaging of organs after *i.v.* injected with DOX@MSN, DOX@MSN@EIN, DOX@Mic, DOX@Mic@EIN and free DOX. (C) Relative tumor volume after treatments. (D) Tumor weights of each group after sacrifice the mice. (E) *Ex vivo* metabonomics analysis of tumors. (F) Frozen slices images of *ex vivo* mouse tumors after the treatment of DOX@MSN, DOX@MSN@EIN, DOX@Mic, DOX@Mic@EIN and free DOX treated mice at the 20th day. (Scale bar: 50 μm) (G) *In vitro* MRI images after the treatment of DOX@MSN, DOX@MSN@EIN, DOX@Mic, DOX@Mic@EIN and free DOX treated mice at the 20th day. (Scale bar: 1 cm).

As shown in Fig. 5B, a sharp fluorescent contrast among tumor sites and main organs was observed. Meanwhile, DOX@MSN@EIN and DOX@Mic@EIN showed higher fluorescence intensity in tumor sites compared with control samples, and DOX@MSN@EIN demonstrated the strongest fluorescence intensity. Liver showed high fluorescence intensity because liver is the organ to filter the blood, detoxifies chemicals and metabolizes drugs *in vivo*. Corresponding to the function of liver, the non-specific uptake of nanoparticles in liver is inevitable. Frozen sections of dissected tumor further confirmed that EIN coated nanomedicines could enhance tumor preferential accumulation of anti-cancer agents (Fig. 5F). These results elucidated that DOX@MSN@EIN and DOX@Mic@EIN could efficiently accumulate in tumor sites. Clinically, it is found that the non-specific inhibition of P-gp usually aggravates side effects due to the compromised drug elimination in liver and kidney. Herein, DOX@MSN@EIN and DOX@Mic@EIN were demonstrated to have a tumor specific accumulation ability, and this strategy was expected to overcome the shortcoming of drug resistance inhibitors.

Thereafter, blood biochemistry was performed (Table S3). As expected, the *i.v.* injection of free DOX significantly increased AST and ALT level, suggesting a serious liver damage. It is noteworthy that the combination of free DOX and EGCG showed an enhanced liver toxicity. However, DOX@MSN@EIN and DOX@Mic@EIN treated mice showed reduced liver toxicity as compared with free drug treated groups. Clearly, our strategy is favorable to overcome the side effects of free drugs.

After post-injection of anti-cancer agents for 20 days, magnetic resonance imaging (MRI) was performed to evaluate the therapeutic efficacy [34]. EIN coated nanomaterials resulted in much smaller tumor sizes compared with control groups, suggesting the enhanced anti-cancer efficacy of EIN coated nanomedicines (Fig. 5G). As summarized in Fig. 5C and D and Fig. S11, on day 25, the reduced tumor volumes further supported that EIN coated nanomedicines could effectively suppress tumor growth without observable body weight loss (Fig. S12). Moreover, H&E staining also confirmed that EIN coated nanomedicines showed excellent therapeutic effect (Fig. 6A) and had negligible toxicity in main organs (Fig. S13). Anti-cancer efficiency was further evaluated by using metabolite analysis. Dissected tumors were homogenized and the supernatant was collected for ^{1}H NMR (Table S4). Main metabolites including lactate, glutathione, taurine, choline, creatine and spermine were analyzed. Relative concentrations of these main metabolites of anti-cancer agents treated mice are illustrated in Fig. 5E. The increased lactate, taurine, spermine and glutathione levels in EIN coated nanomedicines treated samples showed the declined metabolic energy consumption, which corroborated the better therapeutic effects of DOX@MSN@EIN and DOX@Mic@EIN. Furthermore, blood biochemical indexes and blood routine indexes were tested *in vivo* respectively. As shown in Table S5, compared with control group, there were no statistically significant fluctuate in hematology and clinical chemistry parameters in all groups.

After that, the dissected lungs and livers were carefully examined. Compared with the PBS treatment, the treatments of free DOX, DOX@Mic, DOX@MSN, DOX@MSN@EIN and DOX@Mic@EIN resulted reduced macroscopical liver metastasis shown in Fig. 6B and D. As further confirmed by H&E staining in Fig. 6C and E, a very low liver or lung micrometastatic lesion was observed after DOX@MSN@EIN and DOX@Mic@EIN treatments. In contrast, DOX@Mic, DOX@MSN and free DOX displayed obvious metastatic lesions. These results suggested that EIN could efficiently reduce metastasis of highly metastatic cancers [35].

3.6. In vivo drug resistance prevention

Moreover, the capability of EIN coated materials in preventing drug resistance was also studied *in vivo* using immunofluorescence stain (Fig. 7A). The mean fluorescence intensities of the drug efflux associated P-pg, detoxification associated glutathione transferase-π (GST-π) and DNA repair associated topoisomerase-2α (Topo-2α) after different treatments are showed in Fig. 7D. DOX, DOX@MSN and DOX@Mic treated groups displayed increased Topo-2α, GST-π and P-gp expressions, indicating the gaining of drug resistance in tumor cells under chemotherapy. However, the samples treated with EIN-containing agents showed declined expressions in Topo-

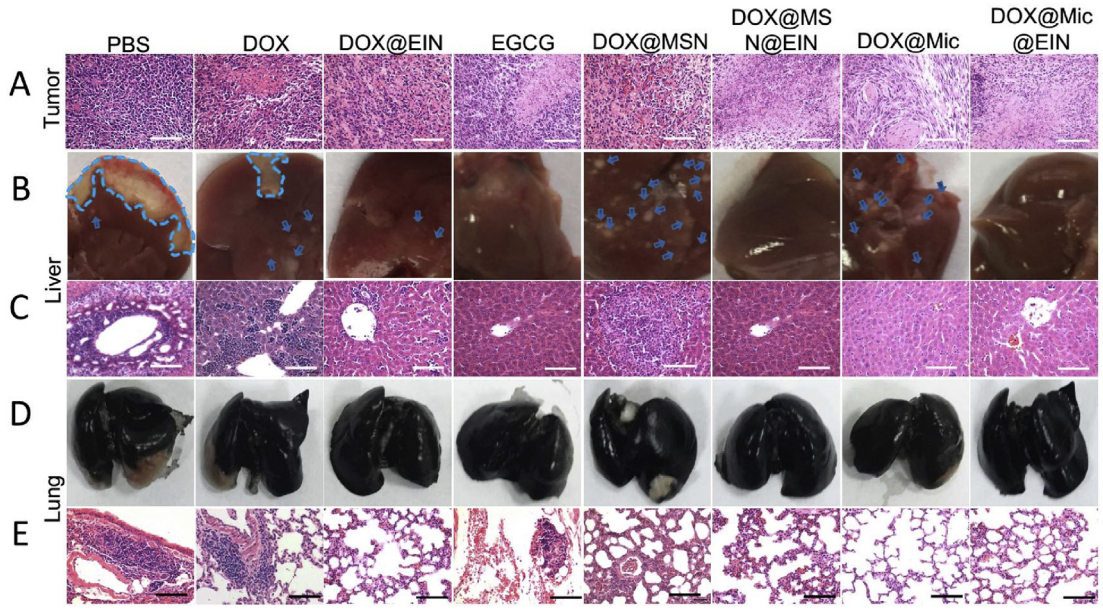

Fig. 6. (A) H&E staining images of tumors after treatment with PBS, DOX, DOX@EIN, EGCG, DOX@MSN, DOX@MSN@EIN, DOX@Mic and DOX@Mic@EIN. (Scale bar: 100 μm) (B–C) Macroscopic and microcosmic images of liver metastasis after treatment with PBS, DOX, DOX@EIN, EGCG, DOX@MSN, DOX@MSN@EIN, DOX@Mic and DOX@Mic@EIN. (Scale bar: 100 μm) (D–E) Macroscopic and microcosmic images of lung metastasis after treatment with PBS, DOX, DOX@EIN, EGCG, DOX@MSN, DOX@MSN@EIN, DOX@Mic and DOX@Mic@EIN. (Scale bar: 100 μm).

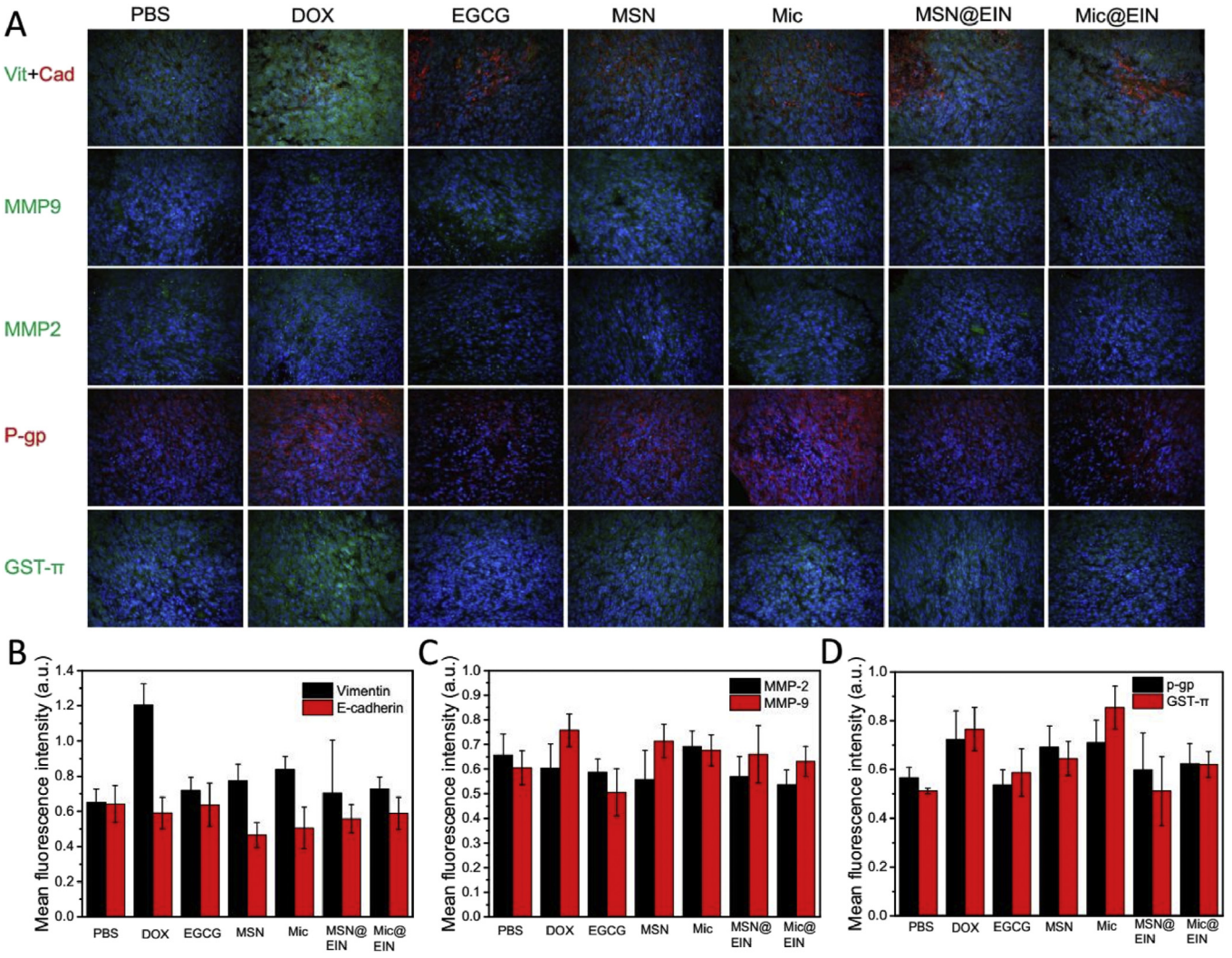

Fig. 7. (A) Immunofluorescence images of vimentin, E-cadherin, MMP-2, MMP-9, P-gp and GST-π. (B) Quantitative analysis of vimentin and E-cadherin. (C) Quantitative analysis of MMP-2 and MMP-9. (D) Quantitative analysis of P-gp and GST-π.

2α, GST-π and P-gp. These results suggested that EIN could potently suppress the development of drug resistance *in vivo*. Next, the *in vivo* anti-metastasis capability of EIN coated nano-platform was evaluated. Since metastasis is started with the degradation of ECM while EMT ensures the successful migration of malignant tumor cells, in this study, ECM degradation associated MMP-2 and MMP-9, and EMT associated vimentin and E-cadherin in tumor site were visualized using immunofluorescence stain (Fig. 7B). When compared with control samples, sections from EIN-containing agents treated mice demonstrated the dimmer fluorescence of MMP-2, MMP-9 and vimentin as well as the brighter fluorescence of E-cadherin (Fig. 7C). Clearly, DOX@MSN@EIN and DOX@Mic@EIN could suppress ECM degradation through inhibiting MMP-2 and MMP-9 expressions and blocking EMT by vimentin and E-cadherin regulations as well, which in turn resulted in the restriction of malignant metastasis.

Encouraged by the favorable therapeutic effect of DOX@MSN@EIN and DOX@Mic@EIN, their anti-cancer capacities were also tested in highly drug resistant MCF-7/ADR tumor bearing mice. As shown in Figs. S14A and S14B, compared with the PBS treated group, free DOX showed minimally tumor suppression ability with a tumor inhibition rate of 13.2%. Besides, DOX@MSN and DOX@Mic groups exhibited moderate therapeutic efficiency with tumor inhibition rates of 52.3% and 54.7%, respectively. Whereas, DOX@MSN@EIN and DOX@Mic@EIN could dramatically improve anti-tumor efficacy with tumor inhibition rates of 78.2% and 73.4%, respectively. Herein, H&E staining also proved that most cancer cells were killed after DOX@MSN@EIN and DOX@Mic@EIN treatments (Fig. S14C_1-C_6). These results demonstrated that EIN coated drug delivery systems could not only prevent cancer cells from gaining drug resistance, but also kill highly drug resistant cancer cells.

4. Conclusion

In summary, by harnessing the capacity of tea polyphenols in tumor progression regulation for various types of cancers, we have engineered EGCG based nano-membrane as a multi-functional nanomedicinal coating to prevent cancer cells from gaining drug resistance and eliminate EMT-type cancer cells to prevent tumor metastasis *in vitro* and *in vivo*. We also demonstrated that, as a versatile coating material, EIN could be coated on different types of conventional nanomedicines to improve their systematic anti-cancer ability. This strategy allows personalized anti-cancer treatments with reduce side effects. Looking forward, this EIN material can be used as a nano-carrier for anti-cancer drugs or as a modification component for drug delivery systems to enhance their

therapeutic efficiency through regulating tumor progression, which is a promising strategy shedding light on the cancer treatments in the future.

Acknowledgements

This work was supported by the National Natural Science Foundation of China (51533006 and 51233003).

Appendix A. Supplementary data

Supplementary data related to this article can be found at http://dx.doi.org/10.1016/j.biomaterials.2017.06.007.

References

[1] D.F. Quail, J.A. Joyce, Microenvironmental regulation of tumor progression and metastasis, Nat. Med. 19 (2013) 1423–1437.
[2] H. Cabral, J. Makino, Y. Matsumoto, P. Mi, H. Wu, T. Nomoto, et al., Systemic targeting of lymph node metastasis through the blood vascular system by using size-controlled nanocarriers, ACS Nano 9 (2015) 4957–4967.
[3] H. Cao, Z. Dan, X. He, Z. Zhang, H. Yu, Q. Yin, et al., Liposomes coated with isolated macrophage membrane can target lung metastasis of breast cancer, ACS Nano 10 (2016) 7738–7748.
[4] N. Aceto, A. Bardia, D.T. Miyamoto, M.C. Donaldson, B.S. Wittner, J.A. Spencer, et al., Circulating tumor cell clusters are oligoclonal precursors of breast cancer metastasis, Cell 158 (2014) 1110–1122.
[5] E. Reategui, N. Aceto, E.J. Lim, J.P. Sullivan, A.E. Jensen, M. Zeinali, et al., Tunable nanostructured coating for the capture and selective release of viable circulating tumor cells, Adv. Mater. 27 (2015) 1593–1599.
[6] D.W. Zheng, B. Li, C.X. Li, J.X. Fan, Q. Lei, C. Li, et al., Carbon-dot-decorated carbon nitride nanoparticles for enhanced photodynamic therapy against hypoxic tumor via water splitting, ACS Nano 10 (2016) 8715–8722.
[7] D.W. Zheng, J.L. Chen, J.Y. Zhu, L. Rong, B. Li, Q. Lei, et al., Highly integrated nano-platform for breaking the barrier between chemotherapy and immunotherapy, Nano Lett. 16 (2016) 4341–4347.
[8] H. Fan, G. Yan, Z. Zhao, X. Hu, W. Zhang, H. Liu, et al., A smart photosensitizer-manganese dioxide nanosystem for enhanced photodynamic therapy by reducing glutathione levels in cancer cells, Angew. Chem. Int. Ed. 55 (2016) 5477–5482.
[9] P. Prasad, C.R. Gordijo, A.Z. Abbasi, A. Maeda, A. Ip, A.M. Rauth, et al., Multifunctional albumin-MnO_2 nanoparticles modulate solid tumor microenvironment by attenuating hypoxia, acidosis, vascular endothelial growth factor and enhance radiation response, ACS Nano 8 (2014) 3202–3212.
[10] R. Straussman, T. Morikawa, K. Shee, M. Barzily-Rokni, Z.R. Qian, J. Du, et al., Tumour micro-environment elicits innate resistance to RAF inhibitors through HGF secretion, Nature 487 (2012) 500–504.
[11] L. Seguin, J.S. Desgrosellier, S.M. Weis, D.A. Cheresh, Integrins and cancer: regulators of cancer stemness, metastasis, and drug resistance, Trends Cell Biol. 25 (2015) 234–240.
[12] C. Holohan, S. Van Schaeybroeck, D.B. Longley, P.G. Johnston, Cancer drug resistance: an evolving paradigm, Nat. Rev. Cancer 13 (2013) 714–726.
[13] C.J. Creighton, X. Li, M. Landis, J.M. Dixon, V.M. Neumeister, A. Sjolund, et al., Residual breast cancers after conventional therapy display mesenchymal as well as tumor-initiating features, Proc. Natl. Acad. Sci. U. S. A. 106 (2009) 13820–13825.
[14] K.R. Fischer, A. Durrans, S. Lee, J. Sheng, F. Li, S.T. Wong, et al., Epithelial-to-mesenchymal transition is not required for lung metastasis but contributes to chemoresistance, Nature 527 (2015) 472–476.
[15] Z. Wang, Y. Li, A. Ahmad, A.S. Azmi, D. Kong, S. Banerjee, et al., Targeting miRNAs involved in cancer stem cell and EMT regulation: an emerging concept in overcoming drug resistance, Drug Resist. Updat 13 (2010) 109–118.
[16] D.K. Lim, R.G. Wylie, R. Langer, D.S. Kohane, Selective binding of C-6 OH sulfated hyaluronic acid to the angiogenic isoform of VEGF(165), Biomaterials 77 (2016) 130–138.
[17] M. Egeblad, Z. Werb, New functions for the matrix metalloproteinases in cancer progression, Nat. Rev. Cancer 2 (2002) 161–174.
[18] B.R. Smith, E.E. Ghosn, H. Rallapalli, J.A. Prescher, T. Larson, L.A. Herzenberg, et al., Selective uptake of single-walled carbon nanotubes by circulating monocytes for enhanced tumour delivery, Nat. Nanotechnol. 9 (2014) 481–487.
[19] B.R. Smith, C. Zavaleta, J. Rosenberg, R. Tong, J. Ramunas, Z. Liu, et al., High-resolution, serial intravital microscopic imaging of nanoparticle delivery and targeting in a small animal tumor model, Nano Today 8 (2013) 126–137.
[20] R. Tong, H.D. Hemmati, R. Langer, D.S. Kohane, Photoswitchable nanoparticles for triggered tissue penetration and drug delivery, J. Am. Chem. Soc. 134 (2012) 8848–8855.
[21] N. Khan, F. Afaq, M. Saleem, N. Ahmad, H. Mukhtar, Targeting multiple signaling pathways by green tea polyphenol (-)-epigallocatechin-3-gallate, Cancer Res. 66 (2006) 2500–2505.
[22] Q. Zhang, D. Wei, J. Liu, In vivo reversal of doxorubicin resistance by (-)-epigallocatechin gallate in a solid human carcinoma xenograft, Cancer Lett. 208 (2004) 179–186.
[23] H. Ejima, J.J. Richardson, K. Liang, J.P. Best, M.P. Van Koeverden, G.K. Such, et al., One-step assembly of coordination complexes for versatile film and particle engineering, Science 341 (2013) 154–157.
[24] M.J. Harrington, A. Masic, N. Holten-Andersen, J.H. Waite, P. Fratzl, Iron-clad fibers: a metal-based biological strategy for hard flexible coatings, Science 328 (2010) 216–220.
[25] H. Kumari, S.R. Kline, C.L. Dennis, A.V. Mossine, R.L. Paul, C.A. Deakyne, et al., Solution-phase and magnetic approach towards understanding iron gall ink-like nanoassemblies, Angew. Chem. Int. Ed. 51 (2012) 9263–9266.
[26] D.W. Zheng, Q. Lei, J.Y. Zhu, J.X. Fan, C.X. Li, C. Li, et al., Switching apoptosis to ferroptosis: metal-organic network for high-efficiency anticancer therapy, Nano Lett. 17 (2017) 284–291.
[27] J.E. Chung, S. Tan, S.J. Gao, N. Yongvongsoontorn, S.H. Kim, J.H. Lee, et al., Self-assembled micellar nanocomplexes comprising green tea catechin derivatives and protein drugs for cancer therapy, Nat. Nanotechnol. 9 (2014) 907–912.
[28] Y. Ping, J. Guo, H. Ejima, X. Chen, J.J. Richardson, H. Sun, et al., pH-responsive capsules engineered from metal-phenolic networks for anticancer drug delivery, Small 11 (2015) 2032–2036.
[29] J.Y. Zhu, Q. Lei, B. Yang, H.Z. Jia, W.X. Qiu, X. Wang, et al., Efficient nuclear drug translocation and improved drug efficacy mediated by acidity-responsive boronate-linked dextran/cholesterol nanoassembly, Biomaterials 52 (2015) 281–290.
[30] H. Kim, H. Okamoto, A.E. Felber, A. Polomska, N. Morone, J.E. Heuser, et al., Polymer-coated pH-responsive high-density lipoproteins, J. Control. Release 228 (2016) 132–140.
[31] N.Y. Frank, A. Margaryan, Y. Huang, T. Schatton, A.M. Waaga-Gasser, M. Gasser, et al., ABCB5-Mediated doxorubicin transport and chemoresistance in human malignant melanoma, Cancer Res. 65 (2005) 4320–4333.
[32] R. Mercado-Lubo, Y. Zhang, L. Zhao, K. Rossi, X. Wu, Y. Zou, et al., A Salmonella nanoparticle mimic overcomes multidrug resistance in tumours, Nat. Commun. 7 (2016) 12225.
[33] C. Yao, P. Wang, X. Li, X. Hu, J. Hou, L. Wang, et al., Near-infrared-triggered azobenzene-liposome/upconversion nanoparticle hybrid vesicles for remotely controlled drug delivery to overcome cancer multidrug resistance, Adv. Mater. 28 (2016) 9341–9348.
[34] W. Yang, W. Guo, W. Le, G. Lv, F. Zhang, L. Shi, et al., Albumin-bioinspired Gd: CuS nanotheranostic agent for in vivo photoacoustic/magnetic resonance imaging-guided tumor-targeted photothermal therapy, ACS Nano 10 (2016) 10245–10257.
[35] W.C. Liao, M. Riutin, W.J. Parak, I. Willner, Programmed pH-responsive microcapsules for the controlled release of CdSe/ZnS quantum dots, ACS Nano 10 (2016) 8683–8689.